Ultrasonic Pulse Velocity Measurements of Cobourg Limestone under Stress

Mark McDonald[1], and Mark Diederichs[1]
[1] *Department of Geological Sciences and Engineering – Queen's University, Kingston, ON, Canada*

ABSTRACT
Ultrasonic pulse velocity (UPV) measurements are conducted by emitting high frequency, acoustic waves through rock core. The velocities of compressional and shear waves (P- and S- waves) are influenced by the unique microstructural characteristics of the tested rock. Using P- and S- wave velocities and bulk density the dynamic elastic material constants such as Young's modulus, Poisson's ratio, shear modulus, and bulk modulus are calculated. As part of the formerly proposed Deep Geologic Repository in southern Ontario, Canada, a site investigation was completed which characterized the geophysical and geomechanical properties of the location. This research presents an analysis of the historical *in situ* field geophysical, and geomechanical data compared to new dynamic testing data. The new dynamic testing is conducted on Cobourg Limestone core under three stress conditions: no compression, uniaxial compression, and confinement stress (hydrostatic). This attempts to replicate simplified stress conditions similar to the *in situ* stresses.

RÉSUMÉ
Les mesures de vitesse des ondes ultrasonores sont effectuées en émettant des ondes acoustiques à haute fréquence à travers d'un cylindre rocheux. La vitesse des ondes de compression et de cisaillement (ondes P- et S-) est influencée par les caractéristiques microstructurales uniques de l'échantillon de roche testé. En utilisant les vitesses d'ondes P- et S- et la densité, les constantes dynamiques du matériau élastique comme le module de Young, le rapport de Poisson, le module de cisaillement et le module de masse peuvent être calculés. Dans le cadre de l'ancien projet de dépôt géologique en profondeur dans le sud de l'Ontario, au Canada, des études de terrains ont été complétés afin de caractériser les propriétés géophysiques et géomécaniques de la masse rocheuse. Cette recherche présente une analyse des données géophysiques et géomécaniques historiques in situ du terrain par rapport à de nouvelles données d'essais dynamiques. De nouveaux essais dynamiques sont effectués sur des spécimens du calcaire de Cobourg sous trois conditions de stress: aucune compression, compression uniaxiale et confinement hydrostatique. On tente ainsi de reproduire des conditions de stress semblables aux conditions in situ.

1 INTRODUCTION

The measurement of ultrasonic pulse velocities (UPV) is a widely used, non-destructive, indirect laboratory testing method for estimating dynamic values of intact rock properties such as Young's modulus (*E*), Poisson's ratio (*v*), shear modulus (*G*), and bulk modulus (*K*) of rock and for evaluating the general quality of the core sample. The method is based on the principle of inducing a pulse and measuring the arrival times of compression (P-) and shear (S-) waves. The respective velocities are estimated based on the time of arrival and the length of the core specimen being tested. However, the elastic constants estimated from UCS test data are considered more representative material parameters and are derived to use in design.

Ultrasonic wave arrival times are also measured *in situ* using advanced geophysical testing tools that can survey the length of the studied borehole. This *in situ* data provides a quantitative and highly detailed continuous record of dynamic rock mass properties. However, with inherent differences present between *in situ* and laboratory dynamic testing, dynamic parameters often vary substantially between testing methods.

In theory, both the laboratory UPV and *in situ* field UPV testing methods provide data for the same parameters and can be compared directly. However, there are numerous factors impacting the difference between laboratory and field acoustic velocity measurements including distance travelled by the pulse wave, sample saturation, stresses acting on the rock mass, wave frequency, medium geometry, borehole wall quality, trace averaging and quality of acoustic coupling between rock core and transducers. Each influencing aspect affects pulse travel times and produces the potential for differences in calculated acoustic velocities between laboratory and borehole acoustic testing methods. These factors must be studied to better understand how to correlate *in situ* and laboratory acoustic velocity measurements.

A review of the methodology for field and laboratory UPV testing is provided in Section 2. A summary of the calculations used for determining acoustic properties and for calculating key dynamic elastic parameters is also provided in Section 2. In Section 3 historical ultrasonic data from laboratory and *in situ* geophysical testing from the formerly proposed Deep Geological Repository in Southern Ontario is summarized (OPG 2019). Testing methods applied in this study are then summarized in Section 4. The historical data is evaluated against new testing data completed at CanmetMINING in Ottawa, Ontario where laboratory UPV measurements were taken under uniaxial and hydrostatic loading conditions in Section 5. Lastly, a discussion regarding the resultant uniaxial and hydrostatic compressed P- wave velocities is presented in Section 6.

2 BACKGROUND

An overview of field and laboratory acoustic testing methods is provided along with an explanation of acoustic wave propagation through rock. This, includes the procedures used to measure wave velocities in the laboratory and *in situ* UPV methods, along with calculations to estimate the elastic constants *E, v, G, and K.*

2.1 Static Moduli

The "static" elastic moduli, E_S, and Poisson's Ratio, v_S, are generally measured from unconfined loading tests on rock cylinders, in accordance with specified standard methods such as ASTM D7012 (ASTM International 2014) or the ISRM Suggested Methods (ASTM International 2008).

2.2 *In situ* Estimation of Dynamic Elastic Constants

In situ borehole acoustic velocity testing is often completed in geotechnical site investigation programs to provide continuous logs of highly detailed acoustic data along the length of a borehole. The acoustic data are then used to calculate dynamic elastic properties along the borehole. A commonly used tool is the full waveform sonic tool which can measure P-, S-, Stoneley, and Tube wave arrivals. As the tool traverses the length of a borehole, the sonic log will record variations in the wave velocities. A simplified schematic of the borehole sonic tool is shown in Figure 1.

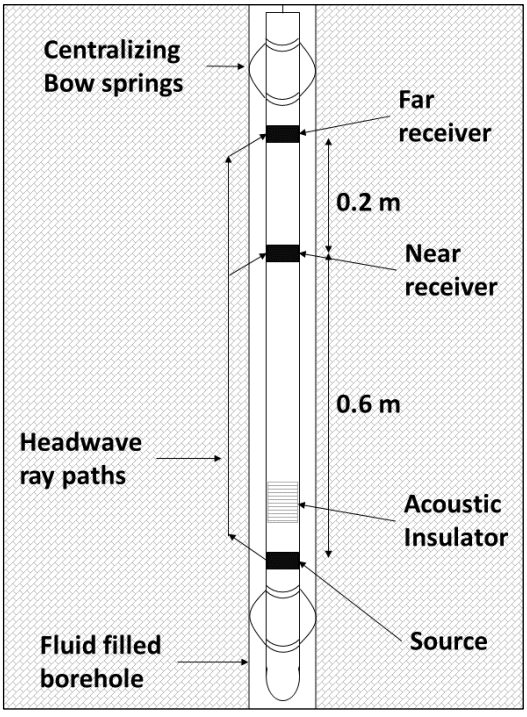

Figure 1: Simplified diagram of a full waveform sonic probe used in borehole acoustic surveys modified from (Paillet and Hon 1991, Agliardi et al. 2016)

Sources waves are generated in the probe by an ultrasonic source, typically operating at 10 - 20 kHz and firing at 0.4 – 20 µs intervals (Paillet and Hon 1991). Multiple receivers (typically two or more) spaced along the tool measure wave arrival times emitted by the transducer. Including multiple receivers in the design of ultrasonic probes allows for the calculation and averaging of acoustic transit times along the borehole. Interval transit time (Δt) is the time required for pulse waves to travel between the receiver(s) divided by receiver spacing. This provides a value of inverse velocity. Inverting interval transit time provides the sonic velocity of the intact rock. Using these *in situ* acoustic velocities, dynamic elastic parameters are calculated.

Sonic tool inputs such as wave frequency, and receiver spacing impact the *in situ* velocity calculations. The selected wave frequency (typically 10-20 Hz) impacts the depth of wave penetration into the surrounding rock mass and the magnitude of wave dispersion. Care must be taken when selecting a source frequency to ensure critically refracted waves penetrate the undisturbed rock mass surrounding the borehole.

Lower acoustic frequencies used in surveys produce greater wave attenuation due to further wave dispersion and therefore result in slower seismic velocities (Toksöz et al. 1981). However, with higher source wave frequencies acoustic resolution increases meaning the impact of small-scale geologic features such as mineral inclusions, fractures, and microcracks will have on the acoustic wave propagation increases. Material heterogeneities which are equal to or larger than the seismic wavelength will refract and disperse seismic waves in a measurable way (Paillet and Hon 1991).

Greater transmitter and receiver spacing impacts wave velocities by increasing the volume of rock mass surveyed and increasing the potential for further wave attenuation. Sonic tools with more than two receiving transducers increase the volume of rock used to calculate the average interval transit time (Δt). In effect this degrades the relative resolution of the acoustic survey compared to laboratory core sampling.

The depth of penetration of critically refracted source waves surrounding the borehole is controlled predominantly by the wavelength of the acoustic signal and the radial velocity distribution. Source frequencies with wavelengths greater than or equal to the borehole diameter ensure critically refracted waves penetrate to a finite depth (Grant and West 1965).

2.3 Laboratory UPV Testing Apparatus

Dynamic elastic constants are measured at the laboratory scale using the UPV method. The UPV testing apparatus (Figure 2) and its components are described below:

- Pulse Generator: The electronic pulse generator produces a voltage output in the form of a rectangular pulse, or gated sine wave.
- Transducers: Consist of a transmitter and receiver which convert electrical pulses to mechanical waves and vice versa.

- Preamplifier: Amplifies weak signals to ensure the receiving transducer can read all signals. It is required when the voltage output of the receiving amplifier is low or if the display and timing units are insensitive.
- Display and timing unit: Voltage pulses applied to the transmitting transducer are displayed on an oscilloscope for visual observation of the waveforms.

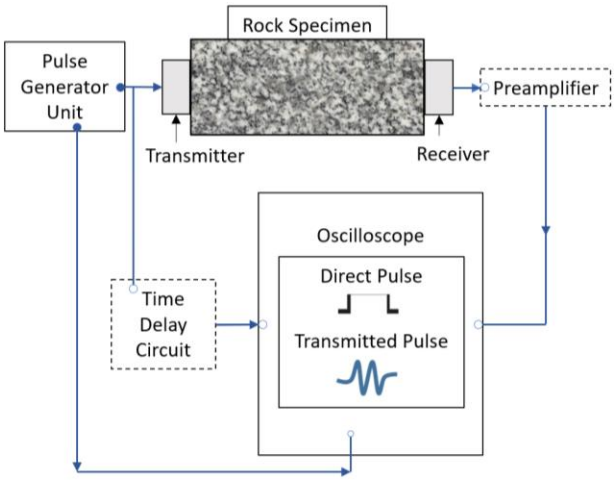

Figure 2. UPV testing set-up modified from (ASTM International 2000)

Figure 3 displays the testing apparatus for the compression UPV system. Hardened steel platens on the top and bottom of the sample serve as the transmitter and receiver for the P- and S- waves while transferring axial load from the UCS machine to the rock core. The GCTS ULT-200 system calculates wave results and displays waveform data on the connected monitor.

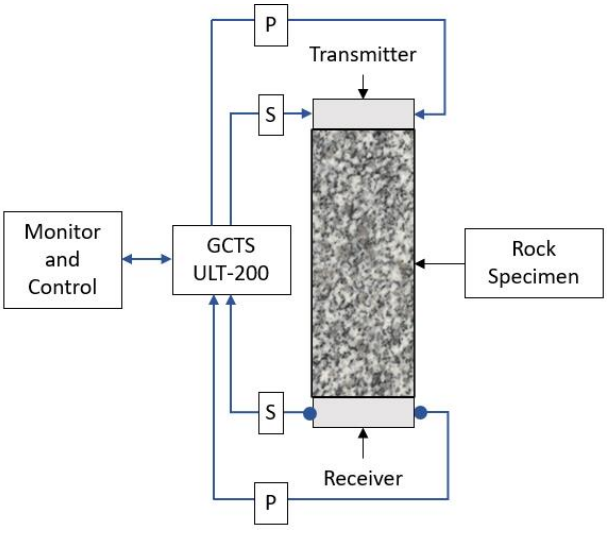

Figure 3. UPV compression testing set-up

2.4 Laboratory UPV Testing Procedure

The positions of the transducers must be centered on each side of the specimen to ensure there is an inclination of two degrees or less between the transducers. The length of each rock core must be measured to produce precise velocity and density calculations. Wave velocity, *v*, is calculated using Equation 1, where *d* is distance and *t* is time. Density, *ρ*, is calculated using Equation 2, where *m* is mass, and *V* is the cylindrical volume of the rock core.

$$v = d/t \quad [1]$$

$$\rho = m/V \quad [2]$$

The optimum voltage level is then determined by increasing voltage output, amplifier gain, and oscilloscope sensitivity, and balancing as necessary to find the level where steeper pulse fronts allow more precise time measurements. The oscilloscope, in conjunction with the time-delay circuit, displays the direct pulse and the first arrival of the transmitted pulse, and measures wave travel time. The counter is triggered to start when the direct pulse is applied to the transmitter and is triggered to stop with the arrival of the first break of a pulse. The first wave to arrive is the compression wave and is detected relatively easily (Figure 4). Shear waves are often difficult to distinguish given the vibrations and reflections of the compression wave. The efficiency of energy transition between the transducers and the rock specimen is improved by using a coupling medium (phenyl salicylate, high vacuum grease, resin). Figure 5 shows an example of a shear wave arrival. Here, the S- wave is taken as the beginning of the waveform where wave amplitude increases significantly. The first wave amplitudes shown in the S- waveform plot is from P- waveforms generated from the diffraction of S-waves at grain boundaries in the rock specimen and are ignored. These refracted P- waveforms are noted by the two dashed red arrows in Figure 5.

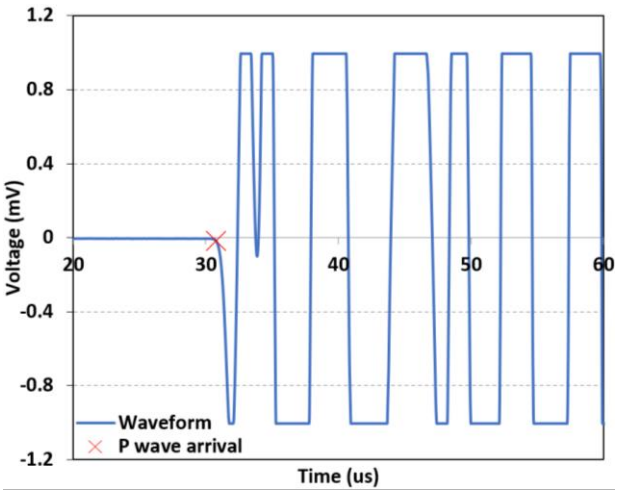

Figure 4: Measurement of a typical P- wave arrival using a plot of time and voltage

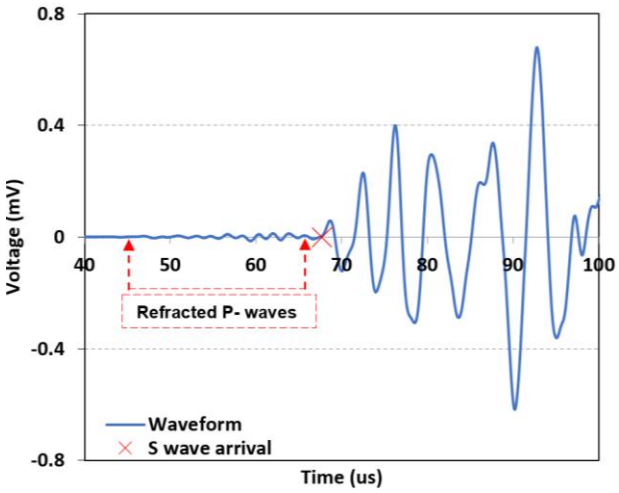

Figure 5: Measurement of a typical S- wave arrival using a plot of time and voltage

2.5 Overview of Acoustic Waves

According to ASTM D2845-08 “Standard Test Method for Laboratory Determination of Pulse Velocities and Ultrasonic Elastic Constants of Rock”, both P- and S- wave velocity arrival times are required to determine the dynamic properties of rock (ASTM International 2014). P- waves travel at speeds ranging from 1-14 km/s in rock and travel through any material, whether solid, liquid, or gas. P-waves are known as push-pull waves since they push and pull against individual waves. This action produces a constant parallel, straight motion. S- waves typically travel at speeds between 1-8 km/s, are transverse waves, meaning they vibrate up and down, perpendicular to the direction of travel and only travel through solid material.

2.6 Dynamic Moduli Calculations

Given the influence of stress and strain on wave propagation, it is not surprising that dynamic elastic moduli are related to acoustic velocities (Mavko et al. 2009). Table 1 below summarizes the dynamic moduli calculations.

Table 1: Summary of dynamic moduli calculations

Elastic Moduli	Equation	Parameters
Bulk Modulus, K	$\rho V_P^2 - \left(\frac{4}{3} V_S^2\right)$	ρ = Density (kg/m^3)
Shear Modulus, G	ρV_s^2	V_P = P- wave velocity (m/s)
General Wave Equation, v	λf	V_S = S- wave velocity (m/s)
Dynamic Young’s Modulus, E_D	$\left(\frac{9KG}{3K+G}\right)$	v = Wave velocity (m/s)
Dynamic Poisson’s Ratio, v_D	$\frac{1}{2}\frac{\left(\frac{V_p}{V_s}\right)^2 - 2}{\left(\frac{V_p}{V_s}\right)^2 - 1}$	λ = Wave amplitude (m)
		f = Wave frequency (Hz)

2.7 Crack Closure, Crack Initiation, Crack Damage Theory and Measurement

Crack closure occurs as microcrack space in the rock specimen is reduced under loading and is observed when the axial stress versus axial strain curve transitions from non-linear to linear behaviour, early on in loading. Crack initiation marks the onset of damage within the rock and can be defined as the point where non-linear lateral strain occurs. Crack damage occurs when axial stress deviates from linear to non-linear behaviour and marks the onset of crack interaction and coalescence. A summary of the methods available for measuring these damage thresholds is given by Diederichs and Martin (2010).

3 HISTORICAL DGR DATA REVIEW

In practice, it is often observed that static elastic properties estimated from laboratory UCS tests do not correlate well to the dynamic elastic constants calculated from UPV measurements.

Laboratory testing was conducted on argillaceous limestone from the Cobourg Limestone formation of the Michigan sedimentary basin to better understand the impact of uniaxial and hydrostatic compression on ultrasonic pulse velocity arrival times of the Cobourg Limestone. Historical data used as part of this study is summarized in this section.

Data from the Ontario Power Generation (OPG) public documents archive were used to determine appropriate average material parameters for static geomechanical properties, laboratory dynamic measurements, and *in situ* geophysical measurements for Cobourg Limestone rock (OPG 2019). This data was collected by or on behalf of OPG as part of its site investigation studies to investigate the feasibility of designing and constructing a formerly proposed deep geologic repository for low and intermediate level nuclear waste in South Bruce Ontario (OPG 2022).

Samples were taken from borehole DGR-6 of the Deep Geological Repository site investigation program located at depths of 760.59 m and 764.34 m. DGR-6 was drilled at an angle of 60° from horizontal (Geofirma Engineering Ltd. 2011a). Figure 6 shows a sample (CR-760.59) of Cobourg Limestone used for testing. All laboratory testing was completed at the CanmetMINING rock mechanics laboratory in Ottawa, ON, Canada.

Figure 6: Cobourg Limestone sample (CR-760.59) used for testing. Sample shown is 83 mm in diameter and 205 mm in length

Cobourg Limestone is classified as a high-strength argillaceous limestone with low permeability and is laterally continuous through southern Ontario and the Michigan sedimentary basin (NWMO 2011). Through extensive laboratory geomechanical testing, Cobourg Limestone was classified as having the average material parameters summarized in Table 2 below.

Table 2: Summary of average Cobourg Limestone material parameters from geomechanical testing (Geofirma Engineering Ltd. 2011a; Engineering Ltd. 2011b; NWMO 2011).

Material Parameter	Cobourg Limestone
Uniaxial Compressive Strength, UCS (MPa)	113
Brazilian Tensile Strength, BTS (MPa)	6.5
Young's Modulus, E_S (GPa)	39
Poisson's Ratio (v_S)	0.3
Crack Initiation Threshold (MPa)	41.4
Crack Damage Threshold (MPa)	88.6

The listed geomechanical parameters are used in the development of UCS and Hoek cell testing parameters and to cross-reference the newly calculated dynamic parameters derived using dynamic laboratory testing methods.

Laboratory dynamic and *in situ* borehole dynamic parameters for the Cobourg Limestone unit are summarized below in Table 3.

Table 3: Summary of average laboratory dynamic moduli values from DGR 1-6 and estimation of average *in situ* dynamic moduli for Cobourg Limestone from DGR-6 using data from Figure 4

Survey Method	P-wave velocity (m/s)	S-wave velocity (m/s)	Dynamic Young's modulus (GPa)
Laboratory UPV	5249	2894	58
Borehole UPV	5700	1800	25

Average *in situ* borehole P- and S- wave velocity values were estimated using the graph of metres length along incline below ground surface (mLBGS) versus velocity (m/s) shown in Figure 7.

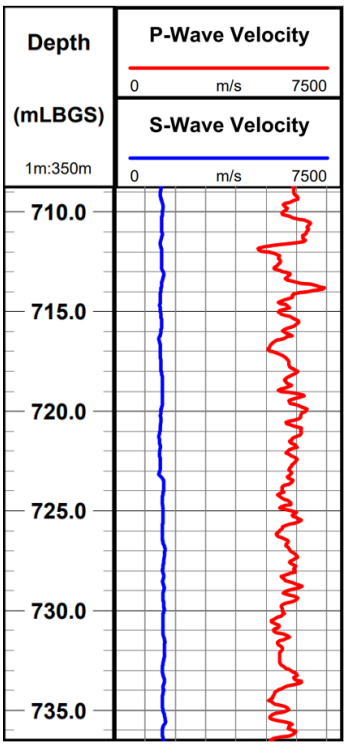

Figure 7: *In situ* P- and S- wave velocities for DGR-6, within the Cobourg Limestone (Geofirma Engineering Ltd. 2011c)

4 TESTING METHODOLOGY AND DATA PROCESSING TECHNIQUES

A summary of UPV uniaxial and hydrostatic compressed testing methods is summarized in this section along with a review of data processing techniques.

4.1 Testing Methodology

Rock core samples were tested under uniaxial compression using the Tinius Olsen 600SL material testing machine. Core samples were cut and ground to a length to distance ratio (L:D) of 2.5 in accordance with ASTM standards for preparing rock core (ASTM International 2019). An annotated diagram of the loading schematic for unconfined compression testing is shown in Figure 8. Figure 9 shows the testing set-up used for hydrostatic compression testing using a Hoek cell. An ENERPAC P393 hydraulic hand pump (not shown) was used to pressurize the Hoek cell. A digital pressure transducer was connected to the hydraulic pump using a LabVIEW program to monitor and store the pressure data digitally (National Instruments Corp. 2022).

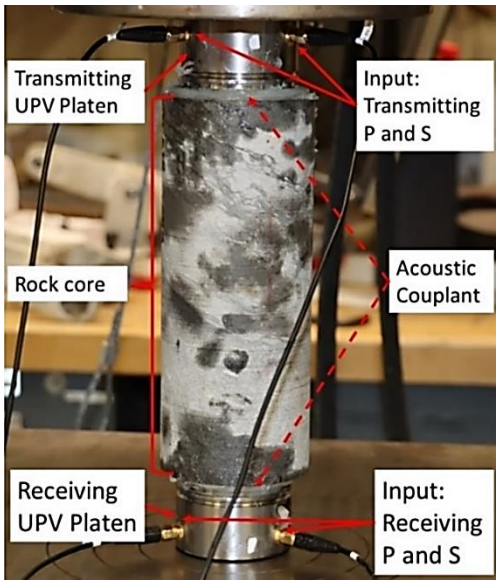

Figure 8: Example ultrasonic compression test set-up for uniaxial compression testing

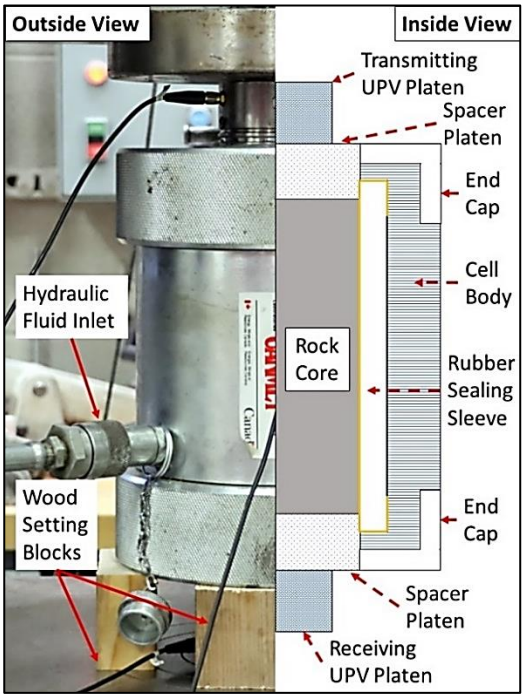

Figure 9: Example set-up of Hoek cell testing. Lefthand side provides an outside view. The righthand side provides a simplified section view. Note: In the outside view, the receiving (bottom) UPV platen is hidden behind the front setting block

In addition to the testing components shown in Figure 8, spherical steel spacer plates were placed between the UPV platens and the rock core. Measurements for P- and S- wave velocities were taken of the two platens before testing to calculate precise delay factors accounting for wave travel time through each platen. Acoustic couplant was applied between all meeting points to ensure efficient wave propagation. A load-controlled program was applied to the Tinius Olsen loading at 2.7 kN/sec. All samples were loaded in the stepwise manner outlined in Table 4 below.

Table 4. Loading steps used with the Tinius Olsen for sample uniaxial loading

Uniaxial loading steps							
Loading Steps	1	2	3	4	5	6	7
Stress (MPa)	0.5	5	10	15	20	25	30
Load (kN)	0.5	26.9	53.7	80.6	107.4	134.3	161.1

Once each load was reached, the machine maintained a constant load until the operator directed the program to move onto the next step. Once step seven of the program was reached, the machine unloaded back to 0 kN at 2.7 kN/sec when directed by the operator. Throughout the sample loading sequence, the GCTS ULT-200 UPV system automatically recorded ultrasonic measurements every 2-10 seconds (depending on the pre-determined input). The program timer was set to 10 min to ensure measurements were recorded for the entirety of the loading sequence. The crystal frequency was set to 1000 kHz for both the P- and S- wave transducers, with waveform stacking set such that 16 wave pulses are emitted during each automatic data acquisition period to reduce noise associated with measurements.

4.2 Data Processing Techniques

UPV data files were exported from the ULT-200 testing machine with the following data: time (sec) of measurement taken, P- and S- wave arrival times (s), and resultant dynamic moduli parameters (v_D, E_D, K, G). Automatic wave arrival selections were checked to ensure correct arrival times are reported. Then, a time delay factor of 13.2 µs and 23.5 µs was subtracted from the reported P- and S- wave arrival times to account for wave travel time through the steel spacer platens. Velocity and loading data from the Tinius Olsen machine were then compiled to align the individual data sets.

5 TESTING RESULTS

Results from UCS, and hydrostatic stress testing are summarized in this section using plots of average P-wave velocity versus stress to present the data.

5.1 Uniaxial Stress Testing

UCS tests were conducted on the Cobourg Limestone sample CR-764.34 to evaluate the impact of uniaxial stress on acoustic velocities. A plot of acoustic velocity versus uniaxial stress test data is shown in Figure 10. These

samples were loaded to a maximum of 30 MPa of stress, approximately 25 % of the maximum compressive strength (as outlined in Section 3.1) to ensure samples were not damaged during testing (NWMO 2011), and equivalent to the maximum vertical overburden stress *in situ* from where the sample was taken. The 7 data points shown in Figure 10 each represent the average value of 19 to 24 P- wave velocity measurements recorded at varied stress levels during three separate loading tests on sample CR-764.34 of Cobourg Limestone.

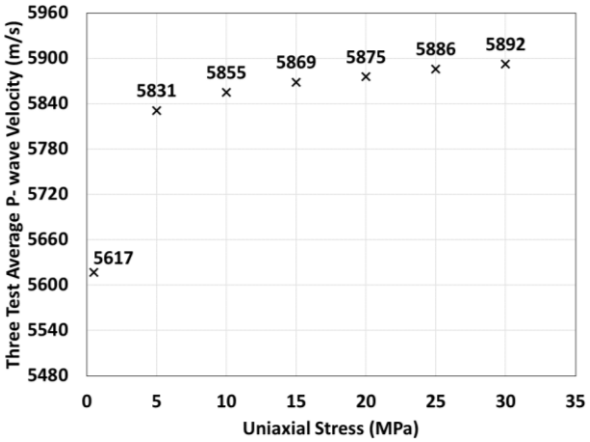

Figure 10: Average P- wave velocity values measured under uniaxial stress for three tests on Cobourg Limestone rock core sample CR-764.34

5.2 Hydrostatic Confining Loads

Hydrostatic stress tests were completed on Cobourg Limestone sample CR-760.59 using a Hoek Cell and Tinius Olsen loading frame. Up to 30 MPa of hydrostatic pressure was applied. Stress versus average P- wave velocities from the test are shown in Figure 11.

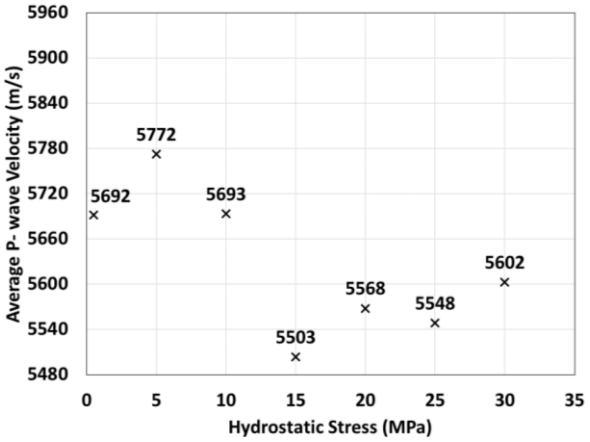

Figure 11: P- wave velocities taken under hydrostatic loading conditions on core sample CR-197

6 DISCUSSION

Shown in Figure 10 are consistent increases in P- wave velocity during unconfined sample loading. Increasing P-wave velocities can be attributed to the microcrack or acoustoelasticity theories (Sayers and King 1990). In the microcrack model of behaviour, stress-induced acoustic velocity changes are impacted by the changing void space of micro-structural features under induced stresses. An increase in velocity is assumed to be the result of microcrack closure from induced stresses. Velocity increases slow down as sample crack closure reduces. In the acoustoelasticity theory, changes from initial wave velocity are attributed to the changing interaction between the acoustic waves and elastic deformation in the rock core (Johnson and Rasolofosaon 1993).

As shown in Figure 11, P- wave velocities appear to have a complex relationship with increasing hydrostatic stress. This complex relationship has been confirmed in studies of acoustic velocities measured under hydrostatic and triaxial stress conditions (Vanorio et al. 2002, Stanchits et al. 2006). During UCS testing as the rock core is loaded in uniaxial compression the material is strained along its core axis and strains unconstrained radially ($\sigma_2 = \sigma_3 = 0$) as a function of its Poisson's ratio. However, in the hydrostatic testing case, confining pressure means the rock core is forced to also expand axially as the entire surface of the core specimen is confined. This is a function of the Poisson's effect (Gercek 2007). Microcrack features in the rock are unable to uniformly compress as in the case of uniaxial compression leading to the initial complex relationship between P- wave velocity and hydrostatic stress.

As shown in the data from Figures 10 and 11, P- wave velocities with a pre-load of 0.2 MPa are similar in magnitude and are only 1.3 % different (acceptable given they are different samples from the same lithology). However, the change in P- wave velocities during hydrostatic loading has a dramatically different behaviour compared to the uniaxial compression test. Here, velocities first increase at 5 MPa of stress, reach a minimum velocity at 15 MPa, then increase consistently until maximum stress is reached at 30 MPa. This behaviour is suspected to be the result of the changing shape and orientations of microcrack features in the rock core. Initial hydrostatic stresses may deform the shape of microcracks leading to increased wave attenuation until crack closure is achieved. With crack closure achieved P- wave velocities should begin to consistently increase with stress until sample crack initiation and crack damage thresholds are reached. Further testing of the Cobourg Limestone beyond 30 MPa should be completed to confirm whether this theory holds true.

6.1 Comparison to *In Situ* Geophysical Data

As demonstrated with P- wave velocity measurements under deviatoric stress conditions, velocities increase sharply with initial loading before crack closure occurs and continue to gradually increase afterwards until sample damage initiates. The difference between *in situ* P- wave measurements and laboratory measurements can be at least partially attributed to the influence of *in situ* stresses on P- wave velocity measurements (Figure 7). The average uniaxial compressed laboratory P- wave velocity at 20 MPa of stress, equivalent to the estimated vertical overburden

stress at 680 metres below ground surface is 5875 m/s. This presents a substantially closer approximation of the average *in situ* borehole P- wave velocity (5700 m/s) compared to the reported unloaded laboratory P-wave velocity of 5249 m/s. However, as outlined in Section 1 many factors affect the resultant differences between each method of UPV measurement excluded from the scope of this research. Correlating between *in situ* and laboratory measurements presents challenges caused by the different lengths of rock, sample damage during handling and drilling, and different wave frequencies used in each method.

7 CONCLUSIONS

Hydrostatic, UCS, and triaxial dynamic testing should be completed under stresses beyond 30 MPa to evaluate the affect of greater stresses on acoustic velocities. Additionally, testing should be completed to quantify the impact of arrival times relative to bedding direction in Cobourg Limestone.

The testing completed in this study demonstrates the influence of stress on P- wave velocities of Cobourg Limestone samples. P- wave velocities increase with uniaxial compression along the core axis. Significant velocity increases occur early on during loading due to microcrack closure. Under hydrostatic stress conditions P-wave velocities exhibited complex behaviour thought to be a function of changing microcrack orientations and shapes.

UPV measurements completed using *in situ* borehole tools provide a continuous record of low-frequency acoustic velocities of the rock mass along the borehole while laboratory dynamic measurements provide high-frequency point measurements of the intact rock core. Measuring acoustic velocities under uniaxial stress magnitudes similar to vertical *in situ* stress reduces the difference between i*n situ* and laboratory acoustic measurements.

ACKNOWLEDGMENTS

The authors thank CanmetMINING for providing laboratory preparation and testing resources essential to complete this research. Thank you to NSERC and NWMO for contributing financial support for this research.

REFERENCES

Agliardi, F., Sapigni, M., and Crosta, G. 2016. Rock Mass Characterization by High-Resolution Sonic and GSI Borehole Logging. *Rock Mechanics and Rock Engineering*, 49: 4303-4318.

ASTM International. 2000. ASTM D2845 - 00 Standard Test Method for Laboratory Determination of Pulse Velocities and Ultrasonic Elastic Constants of Rock. ASTM International, West Conshohocken, PA.

ASTM International. 2008. Standard Test Method for Laboratory Determination of Pulse Velocities and Ultrasonic Elastic Constants of Rock (Withdrawn 2017 (ASTM D2845 - 08). ASTM International, West Conshohocken, PA.

ASTM International. 2014. Test Methods for Compressive Strength and Elastic Moduli of Intact Rock Core Specimens under Varying States of Stress and Temperatures (ASTM D7012-14e1). ASTM International, West Conshohocken, PA.

ASTM International. 2019. ASTM D4543-19 Practices for Preparing Rock Core as Cylindrical Test Specimens and Verifying Conformance to Dimensional and Shape Tolerances. ASTM International, West West Conshohocken, PA.

Diederichs, M.S., and Martin, C.D. 2010. Measurement of spalling parameters from laboratory, *Eurock,* Lausanne Switzerland.

Frederick L Paillet, and Chuen Hon, C. 1991. *Acoustic Waves in Boreholes*. CRC Press Taylor Francis and Group, Boca Raton USA.

Geofirma Engineering Ltd. 2011a. *Drilling, Logging and Sampling of DGR-5 and DGR-6*. Ottawa, ON, CA.

Geofirma Engineering Ltd. 2011b. *Laboratory Geomechanical Strength Testing of DGR-2 to DGR-6 Core*, Ottawa, ON, CA.

Geofirma Engineering Ltd. 2011c. *Drilling, Logging and Sampling of DGR-5 and DGR-6*. Ottawa, ON, CA.

Gercek, H. 2007. Poisson's Ratio Values for Rocks*, International Journal of Rock Mechanics and Mining Sciences*, 44(1): 1–13.

Grant, F.S., and West, G.F. 1965. *Interpretation Theory in Applied Geophysics*. McGraw-Hill, New York, NY, USA.

Johnson, P.A., and Rasolofosaon, P.N.J. 1993. Nonlinear Elasticity and Stress-Induced Anisotropy In Rocks: Reflections On Experimental Results, *1993 SEG Annual Meeting.*

Mavko, G. Mukerji, T. and Dvorkin, J. 2009. *The Rock Physics Handbook: Tools for Seismic Analysis of Porous Media*, 2nd ed., Cambridge Univ. Press.

National Instruments Corp. 2022. LabVIEW. Available from https://www.ni.com/en-ca/shop/labview.html.

NWMO. 2011. *OPG's Deep Geologic Repository, For Low and Intermediate Level Waste, Geosynthesis*.

OPG. 2019. Documents Archive. Available from https://archive.opg.com/. [accessed 9 May 2022].

OPG. 2022. *OPG projects, Deep Geologic Repository*. Available from https://www.opg.com/strengthening-the-economy/our-projects/the-deep-geologic-repository/. [accessed 9 May 2022].

Sayers, C.M., and King, M.S. 1990. Stress-induced Ultrasonic Anisotropy in Berea Sandstone, *International Journal of Rock Mechanics and Mining Sciences & Geomechanics Abstracts, 27: 429-436.*

Stanchits, S., Vinciguerra, S., and Dresen, G. 2006. Ultrasonic Velocities, Acoustic Emission Characteristics and Crack Damage of Basalt and Granite, *Pure and Applied Geophysics*, 163: 975–994.

Toksöz, M.N., Johnston, D.H., and Society of Exploration Geophysicists. 1981. *Seismic wave attenuation. Society of Exploration Geophysicists*, Tulsa, Okla.

Vanorio, T., Prasad, M., Patella, D., and Nur, A. 2002. Ultrasonic Velocity Measurements in Volcanic: Correlation with Microtexture. *Geophysical Journal International*, 149: 22–36.